

Gapless chiral spin liquid in a kagome Heisenberg model

Samuel Bieri,^{1,*} Laura Messio,¹ Bernard Bernu,¹ and Claire Lhuillier¹

¹*Laboratoire de Physique Théorique de la Matière Condensée,
Université Pierre et Marie Curie, CNRS UMR 7600, F-75252 Paris, France*

(Dated: November 6, 2014)

Motivated by recent experiments on the Heisenberg $S = 1/2$ quantum spin liquid candidate material kapellasite, we classify all possible chiral (time-reversal symmetry breaking) spin liquids with fermionic spinons on the kagome lattice. We obtain the phase diagram for the physically relevant extended Heisenberg model, comparing the energies of a wide range of microscopic variational wave functions. We propose that, at low temperature, kapellasite exhibits a novel gapless chiral spin liquid phase with spinon Fermi surfaces. This two-dimensional state inherits many properties of the nearby one-dimensional phase of decoupled anti-ferromagnetic spin chains, but also shows some remarkable differences. We discuss the spin structure factors and other physical properties.

PACS numbers: 75.10.Jm, 75.10.Kt, 75.30.Kz, 75.10.Pq

When low dimensionality, geometric frustration, and anti-ferromagnetism conspire in quantum magnets, completely novel and exotic physics can emerge at low temperature. In such quantum spin liquid (QSL) phases, the picture of classical magnetic moments breaks down, and fractionalized spinon quasi-particles with unusual statistics and long-range entanglement properties become relevant [1]. After intense theoretical research activity on quantum spin liquids in the late 1980s and 90s due to their intimate relation with high-temperature superconductivity [2], interest in QSL has recently regained momentum because of possible applications in quantum computing [3]. More strikingly, however, enormous experimental progress in synthetization and characterization of actual spin liquid candidate materials has catapulted the field to an unprecedented stage of maturity in this century ([4–16] and refs. therein).

A highly interesting recently synthesized QSL candidate material is the so-called kapellasite [14–17]: X-ray diffraction on powder samples of this strong Mott insulator indicates geometrically perfect, uncoupled two-dimensional kagome layers of spin $S = 1/2$ Cu ions, despite some on-site Cu/Zn dilution. Muon spectroscopy shows the absence of frozen moments, inelastic neutron scattering exhibits a continuum of excitations (mimicking a spinon continuum), and the plateau in $1/T_1$ of NMR measurements confirms a fluctuating behaviour down to 20 mK. Experiments on kapellasite therefore provide quite strong evidence in favor of a genuine gapless QSL phase in this material.

In contrast to its polymorph herbertsmithite [12, 13] – one of the best studied QSL candidate to date – kapellasite is known to have important exchange interactions between farther-neighbor sites in the kagome plane [18, 19]. Recent accurate high-temperature series expansion and its fits to susceptibility and specific heat data revealed ferromagnetic interactions on first- and second neighbors, while a dominant anti-ferromagnetic exchange of $J_d \simeq 16$ K is present across the hexagons of the lat-

tice [16, 17]. These results open up exciting new theoretical prospects, because *classical* spin models on the kagome lattice with such farther-neighbor interactions are known to exhibit *non-planar* Néel phases, i.e., a spontaneous breaking of time-reversal symmetry (TRS) [20]. Whether such chiral symmetry breaking can carry over to the quantum regime in a spin liquid phase is one of the central questions we want to address in this paper. Ideas for chiral spin liquids (CSL) were presented some time ago [21–23], but despite the initial excitement and intense research efforts, the lack of realistic theoretical models and experimental realizations of such exotic phases finally lead to a stagnation in activity. Recently, however, DMRG computations on a farther-neighbor kagome anti-ferromagnet found evidence for a gapped CSL state [24].

In this paper we present a phase diagram of the extended quantum Heisenberg model on the kagome lattice,

$$H = J_1 \sum_{\langle i,j \rangle} \mathbf{S}_i \cdot \mathbf{S}_j + J_2 \sum_{\langle\langle i,j \rangle\rangle} \mathbf{S}_i \cdot \mathbf{S}_j + J_d \sum_{\langle i,j \rangle_d} \mathbf{S}_i \cdot \mathbf{S}_j \quad (1)$$

with ferromagnetic interactions on first and second neighbors ($J_1 \leq 0$, $J_2 \leq 0$), and anti-ferromagnetic interaction $J_d \geq 0$ across the diagonals of the hexagons [25]. Testing an exhaustive set of microscopic spin liquid and correlated Néel wave functions, we find the variational phase diagram presented in Fig. 1. In the inset, the phase diagram for the corresponding classical spin model is displayed. The phase dubbed $\sqrt{3} \times \sqrt{3}$ has a planar order and a 9-site cell, while cuboc-1 and cuboc-2 have non-planar spins in a 12-site cell [20]. For $J_d \gtrsim 0.5$, we find three new types of QSL phases: a dimensionally reduced, quasi-1D and two TRS breaking phases. We elaborate on these results in the remainder of the paper.

Néel ordered states. Due to the presence of ferromagnetic couplings which favor local transient creation of spin $> 1/2$, it can be suspected that semi-classical Néel phases can survive in large parts of the phase diagram. Black symbols in Fig. 1 designate points where long-range

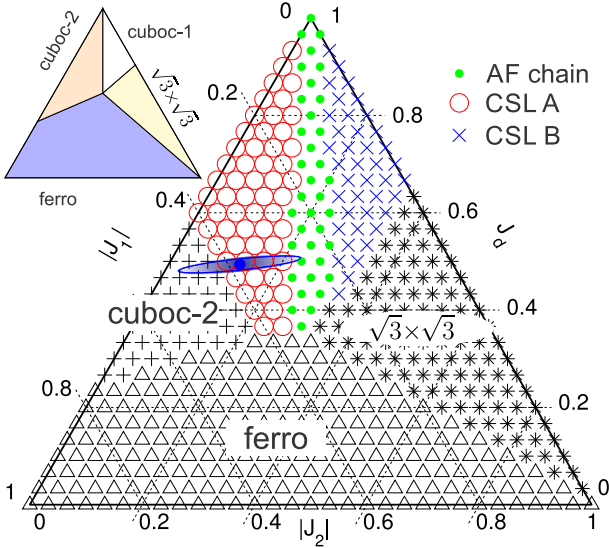


FIG. 1. Quantum phase diagram of model (1) for $J_d \geq 0$ and $J_1, J_2 \leq 0$, with $|J_1| + |J_2| + J_d = 1$. Horizontal lines are $J_d = \text{cst.}$ The blue area represents parameters best describing kapellasite [17]. Left inset: classical phase diagram.

ordered states have the lowest energy. We obtain these wave functions by the Huse-Elser construction [26],

$$|\text{Neel}\rangle = e^{-\sum_{i,j} J_{ij} S_i^z S_j^z} \prod_j |S\rangle_j, \quad (2)$$

i.e., non-trivial quantum fluctuation is introduced in product states of classical spin orders by first-, second-, and diagonal-neighbor Jastrow factors. This class of wave functions is known to give excellent variational estimates of the ground-state energy for ordered quantum spin systems [26, 27].

QSL wave functions. Since the putative spin liquid in kapellasite has gapless excitations, we choose to fractionalize spin into fermionic spinon operators $(f_\alpha) = (f_\uparrow, f_\downarrow)$ as $2S^a = f_\alpha^\dagger \sigma_a^{\alpha\beta} f_\beta$, where σ_a are Pauli matrices. This spin representation introduces a gauge redundancy $\psi = (f_\uparrow, f_\downarrow)^T \mapsto g\psi$, where g is any $\text{SU}(2)$ matrix. The state is then constructed via a quadratic spinon Hamiltonian

$$H_0 = \sum_{ij} \xi_{ij} f_{i\alpha}^\dagger f_{j\alpha} + \Delta_{ij} [f_{i\uparrow} f_{i\downarrow} - f_{i\downarrow} f_{i\uparrow}] + \text{h.c.}, \quad (3)$$

and the microscopic wave function is its Gutzwiller-projected ground state $|\text{QSL}\rangle = \prod_j n_j (2 - n_j) |\psi_0\rangle$ [28, 29]. Note that for chiral spin liquids, the parameters ξ_{ij} and Δ_{ij} are complex in general. At the level of the effective mean-field theory, the $\text{SU}(2)$ gauge redundancy is generically broken down to $\text{U}(1)$ or \mathbb{Z}_2 . The theoretical challenge is to exhaustively enumerate all possible liquid phases of the form (3) that follow certain symmetry requirements. For this we use the projective symmetry group (PSG) approach introduced by Wen [30], and subsequently applied to the kagome lattice in [31, 32].

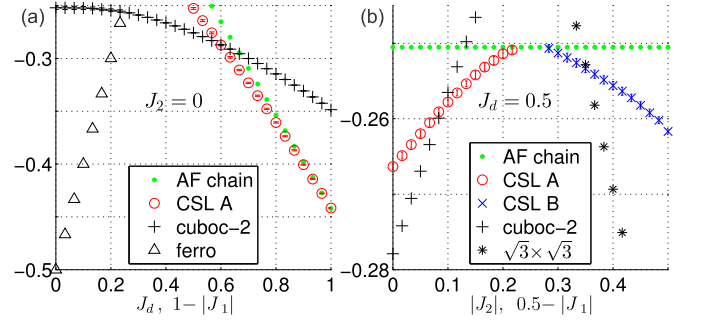


FIG. 2. Variational energy of microscopic w.f. on the lines $J_2 = 0$ (a) and $J_d = 0.5$ (b) of the phase diagram.

In this paper, we significantly extend previous results by systematically classifying time-reversal symmetry broken fermionic QSL phases on the kagome lattice. We are interested in phases with unbroken translation and spin rotation symmetries. The CPT theorem implies that breaking of time-reversal is accompanied by breaking of a reflection symmetry. The kagome lattice has a $\pi/3$ rotation symmetry R , and reflection symmetries σ and σ' , related by $R\sigma = \sigma'$. We therefore find three possible ways how TRS can break on this lattice: (a) R is intact, and all reflection symmetries σ and σ' are broken; (b) R and σ are broken, σ' is intact; (c) R and σ' are broken, σ is intact [33]. We label these three types of chiral symmetry breaking by $(\tau_\sigma, \tau_R) = (1, 0)$, $(1, 1)$, and $(0, 1)$, respectively. The fourth case $(\tau_\sigma, \tau_R) = (0, 0)$ corresponds to “symmetric” spin liquids, i.e., unbroken TRS [31]. Classical spin states with these symmetries are (a) octahedral state, (b) cuboc-1, and (c) cuboc-2 [20].

The algebraic PSG is a projective representation of the lattice symmetries in the $\text{SU}(2)$ gauge group [30]. We find that this representation is not affected by the type of TRS breaking discussed above, and thus there remain 20 gauge inequivalent classes of algebraic PSGs [31] in the chiral case. However, at the level of mean fields $\{\xi_{ij}, \Delta_{ij}\}$ compatible with the symmetries, time-reversal plays a crucial role and introduces strong constraints on their possible values. In this paper, we focus on phases where non-zero mean fields are allowed on *at least two* out of first, second, and diagonal links of the kagome lattice. Mean-fields on all other links are set to zero. This choice is motivated by the spin model (1) we want to study. Given these restrictions, we find in total 25 distinct chiral mean-field phases (3) with a \mathbb{Z}_2 gauge structure. We leave a detailed investigation of these \mathbb{Z}_2 QSLs for future work. Instead, we focus on phases where the mean-field gauge group is $\text{U}(1)$. We find 15 such $\text{U}(1)$ QSL phases, listed in Tab. I. The first two columns in this table specify the type of TRS breaking. Thus, phases no. 1 and 2 are symmetric liquids with unbroken TRS. Phases 3 to 15 break time reversal. Columns 3, 4, and 5 specify the algebraic PSG, i.e., the $\text{SU}(2)$ representation of lattice translation, re-

no	τ_σ	τ_R	ϵ_2	g_σ	g_R	β_1	β_2	β_d	Description
1	0	0	+	$\mathbb{1}_2$	$\mathbb{1}_2$	0	0	0	large Fermi surface
2	0	0	-	$\mathbb{1}_2$	$\mathbb{1}_2$	0	0	x	Dirac spect. [34]
3	1	1	+	$\mathbb{1}_2$	$\mathbb{1}_2$	0	$\pi/2$	x	triangular FS
4	1	1	+	$i\sigma_2$	$i\sigma_2$	0	β_2	0	large FS
5	1	1	-	$\mathbb{1}_2$	$\mathbb{1}_2$	0	$\pi/2$	0	Dirac spectrum
6	1	1	-	$i\sigma_2$	$i\sigma_2$	0	β_2	x	FS/Dirac
7	0	1	+	$\mathbb{1}_2$	$\mathbb{1}_2$	$\pi/2$	0	$\pi/2$	triangular FS
8	0	1	+	$\mathbb{1}_2$	$i\sigma_2$	β_1	0	β_d	large FS
9	0	1	-	$\mathbb{1}_2$	$\mathbb{1}_2$	$\pi/2$	0	x	kagome FS
10	0	1	-	$\mathbb{1}_2$	$i\sigma_2$	β_1	0	x	FS/Dirac
11	0	1	-	$i\sigma_2$	$\mathbb{1}_2$	β_1	x	0	Dirac spectrum
12	1	0	+	$i\sigma_2$	$\mathbb{1}_2$	β_1	β_2	0	large FS
13	1	0	-	$i\sigma_2$	$i\sigma_2$	$\pi/2$	β_2	$\pi/2$	CSL A
14	1	0	-	$\mathbb{1}_2$	$i\sigma_2$	β_1	$\pi/2$	β_d	CSL B
15	1	0	-	$i\sigma_2$	$\mathbb{1}_2$	β_1	β_2	$\pi/2$	fully gapped

TABLE I. QSL phases with U(1) gauge structure, including symmetric ($\tau_\sigma, \tau_R = 0$) and chiral ($\tau_\sigma = 1$ or $\tau_R = 1$) liquids [35]. $\epsilon_2 = -1$ indicates doubling of the spinon unit cell. $\beta_a = \arg(\xi_a)$ are the allowed hopping phases in (3); “x” means $\xi_a = 0$.

flection, g_σ , and $\pi/3$ rotation symmetry, g_R . We work in a gauge where the representation of x -translation is trivial, $g_x = \mathbb{1}_2$; the y translation is staggered according to the sign ϵ_2 , $g_y = (\epsilon_2)^x \mathbb{1}_2$. Similar to the U(1) PSG representation for bosonic spinons [36, 37], we can show that there is always a gauge where the point group representations are independent of sublattice site. Furthermore, for U(1) liquids $\Delta_{ij} = 0$ without loss of generality. Finally, columns β_1 , β_2 , and β_d in Tab. I contain the allowed complex phases of first, second, and diagonal mean-fields ξ_a ; “x” indicates that hopping must vanish by symmetry, $\xi_a = 0$; β_a means the phase is unconstrained. If allowed by symmetry, the relative hopping amplitudes, signs, and complex phases are free and will be used as variational parameters [33]. In the last column we give some robust properties of these phases [35], but more details will be published elsewhere.

Quantum phase diagram. Using large-scale Monte Carlo calculations, we determine the optimal parameters minimizing the energy of (1) in the correlated Néel (2) and in the chiral U(1) QSL wave functions (3). The resulting phase diagram is shown in Fig. 1. The energies of the best variational states on the lines $J_2 = 0$ and $J_d = 0.5$ are given in Fig. 2. Black symbols in these figures represent long-range ordered phases [38]. As expected, when J_1 and J_2 are dominant, the system is a ferromagnet. When the strength of J_d increases, it exhibits a first-order transition to semi-classical Néel phases, either of non-planar cuboc-2 type or with planar $\sqrt{3} \times \sqrt{3}$ order, depending on the relative strengths of J_1 and J_2 . With even larger J_d , the ground state moves to true QSL phases (color symbols online). At $J_d = 1$, the model consists of decoupled anti-ferromagnetic (AF) chains. The

AF chain is a well-known QSL with gapless Fermi points of deconfined spinons. In our approach, this phase is represented by the so-called “Gutzwiller-RVB” wave function [39] – a projected chain of itinerant fermions – which is known to be an extremely good approximation to the true ground state. Surprisingly, as we decrease J_d while keeping $J_1 \simeq J_2$, the 1D phase is very robust and it remains the lowest state. This dimensional reduction can be understood if we picture the chains as AF ordered classical spins: inter-chain couplings induced by non-zero $J_1 = J_2$ exactly cancel, and 2D correlations do not lower the energy. For $|J_1| \gtrsim 2|J_2|$ and $|J_1| \lesssim |J_2|/2$, however, we find truly two-dimensional chiral spin liquid phases, no. 13 and 14 in Tab. I, respectively. In the classical model, $J_1 = J_2$ is a line of first-order transition from chiral cuboc-2 to cuboc-1 phases. In the quantum case, our results indicate the existence of an extended intermediate phase with essentially 1D character. This phase may give birth to two-dimensional spin liquids through second-order phase transitions, and the presence of quantum critical lines seems plausible.

Chiral spin liquids. Let us discuss the nature of the found 2D QSL states in more detail. We denote the phase for dominant J_1 by CSL A, and the one for dominant J_2 by CSL B. Both are gapless with spinon Fermi surfaces, and they break reflection and TRS, while all other model symmetries are intact. For definiteness, we give the optimal variational parameters at $J = (|J_1|, |J_2|, J_d) = (0.4, 0.1, 0.5)$ for CSL A, and at $J = (0.1, 0.3, 0.6)$ for CSL B. The hopping amplitudes for CSL A are $\xi = (|\xi_1|, |\xi_2|, |\xi_d|) \simeq (0.2, 2.7, 7.1)$; the complex hopping phases on first-neighbor and diagonal links are fixed to $\pi/2$ by symmetry (see no. 13 in Tab. I), and we find $\beta_2 \simeq \pi/5$ for the optimal phase on the second-neighbor link. For CSL B, we find $\xi \simeq (2.4, 0.2, 7.4)$. Here, the complex phases on first and diagonal links are free (see no. 14), and we find the optimal values $\beta_1 \simeq \pi/5$ and $\beta_d \simeq -\pi/25$. QSLs are conveniently characterized by gauge invariant fluxes piercing loops of lattice links [30, 40, 41]. Using the PSG in Tab. I, CSL A thus has a U(1) flux $\simeq 2\pi/5$ through triangles of second-neighbor links. On the other hand, CSL B exhibits a flux $\simeq 2\pi/5$ through small lattice triangles and no flux pierces the hexagons. Note that the optimal hopping phases (and hence the fluxes) on second and first neighbors are simply exchanged in CSL A and CSL B [42].

Static structure factor. In Fig. 3, we display the static spin structure factor $S(\mathbf{q})$ for the three QSL phases calculated on square clusters of $N = 3(12)^2$ sites [33]. In the 1D phase for $J_1 \simeq J_2$, the spinon can only propagate along the diagonals of the hexagons, which form arrays of uncoupled chains in three directions \hat{e}_1 , \hat{e}_2 , and \hat{e}_3 . The structure factor for these chains is logarithmically divergent in N at momenta connecting the Fermi points, determined by $\mathbf{q} \cdot \hat{e}_n = \pi/(2a)$; (nearest-neighbor distance $a = 1$). This explains the lines of intensity in the

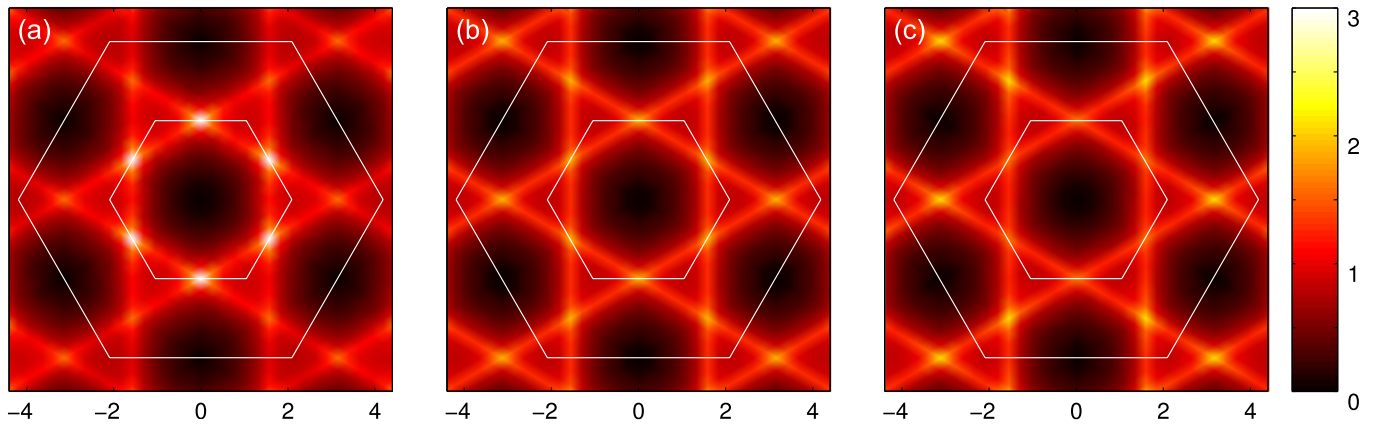


FIG. 3. Static spin structure factor $S(\mathbf{q})$ in the phases CSL A (a), AF chain (b), and CSL B (c).

1D phase Fig. 3b. When moving to the 2D CSL phases in Figs. 3a and 3c, these general geometric features of $S(\mathbf{q})$ remain. However, the scattering becomes more diffuse, and the passage to 2D is accompanied by a transfer of spectral weight. In CSL A, the intensity is concentrated at the six inner line crossings (M points), while in CSL B, it is dominantly at the outer crossings. This is a fading reminiscence of soft points in the classical partners of these phases [20].

Physical properties. The blue area in Fig. 1 depicts the confidence region of model parameters describing kapellasilite according to recent experimental fits [17]. The most likely spin exchange for this material is located in the CSL A phase. The presence of maxima in $S(\mathbf{q})$ at the M points (Fig. 3a) is in excellent agreement with recent neutron scattering data on powder samples [16]. However, this comparison cannot be exhaustive as we are not able to reliably calculate the dynamical structure factors. Nevertheless, we can construct projected $S = 1$ excitations above the ground state [34] in this phase. We confirm the existence of gapless excitations near the Fermi surfaces, and we estimate the spinon bandwidth as ~ 2.1 meV in the thermodynamic limit, in good agreement with experiment. The weak reinforcement of scattering signal at small wave vector q (see Fig. 1 of Ref. [16] for $q \simeq 0.15 \text{ \AA}^{-1}$ and $\omega \simeq 0.2$ meV) may seem inconsistent with our theory. However, the presence of non-magnetic Zn impurities in the material ($\sim 27\%$) can account for this: The AF chains – at the origin of stability for the QSL phases – are reduced in length by impurities. Odd-size chains act similar to orphan moments [43] which, in our model, couple ferromagnetically. We believe this effect is responsible for the low- q signal seen in experiment.

The found gapless CSLs are expected to exhibit longitudinal spin and heat transport [44]. Furthermore, spontaneous TRS breaking implies corresponding Hall currents, even in the absence of Dzyaloshinskii-Moria terms or external magnetic fields. Classical simulations sug-

gested that chiral symmetry breaking can survive up to small but finite temperature [45]. A naive mean-field calculation for our CSL phases predicts a linear temperature scaling of specific heat and conductivities, but strong spinon interaction due to U(1) gauge fluctuation is likely to change this result [46]. Nevertheless, a non-zero Hall angle is robust and would be a strong experimental indication in favor of our theory.

Conclusion. In this paper we studied the zero-temperature phase diagram of the quantum Heisenberg model (1) on the kagome lattice with ferromagnetic exchanges J_1 and J_2 , and anti-ferromagnetic J_d across the hexagons. It harbors not only semi-classical phases, but also genuine chiral spin liquids. On this basis, we propose a quantitative explanation for the scattering pattern measured in powder samples of kapellasilite, and we predict the structure factor expected for single crystals. From a theoretical perspective, these CSLs appear through frustration of arrays of AF spin chains. It is a rare occurrence of TRS breaking in a pure Heisenberg model without higher-order spin exchange [47–49]. This opens interesting avenues for other approaches (1D bosonization [50], DMRG [51–56], DMFT [57], fRG [58], cluster methods [59, 60], refined VMC [61–63], etc) exploring this novel type of dimensional crossover from 1 to 2D quantum phases. In fact, compounds with a network of frustrated AF chains are ubiquitous and their neutron diffraction patterns remain *terra incognita*.

We thank P. Mendels, B. Fåk, F. Bert, M. Serbyn, and P. A. Lee for many helpful discussions. The supercomputer “Mesu” of UPMC and the computing cluster of LPTMC were used for the numerical results. UPMC belongs to Sorbonne Universités. This work is supported by ANR-12-BS04-0021.

* samuel.bieri@alumni.epfl.ch

- [1] L. Balents, *Nature* **464**, 199 (2010); P. A. Lee, *Science* **321**, 1306 (2008).
- [2] P. A. Lee, N. Nagaosa, and X.-G. Wen, *Rev. Mod. Phys.* **78**, 17 (2006).
- [3] A. Kitaev, *Annals of Physics* **321**, 2 (2006).
- [4] R. Coldea, D. A. Tennant, A. M. Tsvelik, and Z. Tylczynski, *Phys. Rev. Lett.* **86**, 1335 (2001).
- [5] S. Yamashita *et al.*, *Nat. Phys.* **4**, 459 (2008).
- [6] T. Itou *et al.*, *Nat. Phys.* **6**, 673 (2010).
- [7] H. D. Zhou *et al.*, *Phys. Rev. Lett.* **106**, 147204 (2011).
- [8] J. G. Cheng *et al.*, *Phys. Rev. Lett.* **107**, 197204 (2011).
- [9] A. Zorko *et al.*, *Phys. Rev. Lett.* **101**, 026405 (2008).
- [10] H. D. Zhou *et al.*, *Phys. Rev. Lett.* **109**, 267206 (2012).
- [11] T.-H. Han *et al.*, *Nature* **492**, 406 (2012).
- [12] J. S. Helton *et al.*, *Phys. Rev. Lett.* **98**, 107204 (2007).
- [13] P. Mendels *et al.*, *Phys. Rev. Lett.* **98**, 077204 (2007).
- [14] R. H. Colman, C. Ritter, and A. S. Wills, *Chem. Mater.* **20**, 6897 (2008); R. Colman, A. Sinclair, and A. Wills, *Chem. Mater.* **22**, 5774 (2010).
- [15] E. Kermarrec *et al.*, *Phys. Rev. B* **90**, 205103 (2014).
- [16] B. Fåk *et al.*, *Phys. Rev. Lett.* **109**, 037208 (2012).
- [17] B. Bernu, C. Lhuillier, E. Kermarrec, F. Bert, P. Mendels, R. H. Colman, and A. S. Wills, *Phys. Rev. B* **87**, 155107 (2013).
- [18] O. Janson, J. Richter, and H. Rosner, *Phys. Rev. Lett.* **101**, 106403 (2008).
- [19] H. O. Jeschke, F. Salvat-Pujol, and R. Valentí, *Phys. Rev. B* **88**, 075106 (2013).
- [20] L. Messio, C. Lhuillier, and G. Misguich, *Phys. Rev. B* **83**, 184401 (2011).
- [21] V. Kalmeyer and R. B. Laughlin, *Phys. Rev. Lett.* **59**, 2095 (1987); *Phys. Rev. B* **39**, 11879 (1989).
- [22] X. G. Wen, F. Wilczek, and A. Zee, *Phys. Rev. B* **39**, 11413 (1989).
- [23] K. Yang, L. K. Warman, and S. M. Girvin, *Phys. Rev. Lett.* **70**, 2641 (1993).
- [24] S.-S. Gong, W. Zhu, and D. N. Sheng, *Sci. Rep.* **4**, 6317 (2014).
- [25] We choose an energy scale such that $|J_1| + |J_2| + J_d = 1$ throughout this paper.
- [26] D. A. Huse and V. Elser, *Phys. Rev. Lett.* **60**, 2531 (1988).
- [27] L. Capriotti, A. E. Trumper, and S. Sorella, *Phys. Rev. Lett.* **82**, 3899 (1999).
- [28] C. Gros, *Annals of Physics* **189**, 53 (1989).
- [29] S. Bieri, M. Serbyn, T. Senthil, and P. A. Lee, *Phys. Rev. B* **86**, 224409 (2012).
- [30] X.-G. Wen, *Phys. Rev. B* **65**, 165113 (2002).
- [31] Y.-M. Lu, Y. Ran, and P. A. Lee, *Phys. Rev. B* **83**, 224413 (2011).
- [32] T. Dodds, S. Bhattacharjee, and Y. B. Kim, *Phys. Rev. B* **88**, 224413 (2013).
- [33] See Supplemental Material for more detailed information.
- [34] Y. Ran, M. Hermele, P. A. Lee, and X.-G. Wen, *Phys. Rev. Lett.* **98**, 117205 (2007); M. Hermele *et al.*, *Phys. Rev. B* **77**, 224413 (2008).
- [35] Some of the QSL states in Tab. I (albeit only for first neighbors) have been discussed previously [34, 64, 65]. We ignore states with flat bands at the Fermi energy, for which there is no unique ground state. Clearly, all states develop Fermi surfaces when ξ_d becomes dominant.
- [36] F. Wang and A. Vishwanath, *Phys. Rev. B* **74**, 174423 (2006).
- [37] L. Messio, C. Lhuillier, and G. Misguich, *Phys. Rev. B* **87**, 125127 (2013); L. Messio, B. Bernu, and C. Lhuillier, *Phys. Rev. Lett.* **108**, 207204 (2012).
- [38] QSL states are calculated on square clusters of $N = 3(12)^2$ sites. Such large systems are necessary especially when $|\xi_d| \gg |\xi_1|, |\xi_2|$ and finite-size effects become strong. Spinon boundary conditions are periodic in one, anti-periodic in the other lattice direction. The ordered w.f. are mostly calculated on $N = 3(24)^2$ sites. We use thermodynamic energies for the 1D phase [39].
- [39] B. S. Shastry, *Phys. Rev. Lett.* **60**, 639 (1988); F. D. M. Haldane, *Phys. Rev. Lett.* **60**, 635 (1988).
- [40] Y. Iqbal, F. Becca, and D. Poilblanc, *Phys. Rev. B* **83**, 100404 (2011).
- [41] B. K. Clark *et al.*, *Phys. Rev. Lett.* **111**, 187205 (2013).
- [42] Accurate determination of parameters is difficult in Monte Carlo, because energies (and other physical properties) weakly depend on them. In some cases we find slightly different fluxes with almost degenerate energy. However, TRS breaking appears to be robust.
- [43] L. Thompson and P. A. Lee, arXiv:1202.5655.
- [44] H. Katsura, N. Nagaosa, and P. A. Lee, *Phys. Rev. Lett.* **104**, 066403 (2010).
- [45] J.-C. Dörmge, C. Lhuillier, L. Messio, L. Pierre, and P. Viot, *Phys. Rev. B* **77**, 172413 (2008); L. Messio *et al.*, *Phys. Rev. B* **78**, 054435 (2008).
- [46] O. I. Motrunich, *Phys. Rev. B* **72**, 045105 (2005); *Phys. Rev. B* **73**, 155115 (2006).
- [47] A. Läuchli, G. Schmid, and M. Troyer, *Phys. Rev. B* **67**, 100409 (2003).
- [48] R. V. Mishmash, J. R. Garrison, S. Bieri, and C. Xu, *Phys. Rev. Lett.* **111**, 157203 (2013).
- [49] A. E. B. Nielsen, G. Sierra, and J. I. Cirac, *Nat. Commun.* **4**, 2864 (2013).
- [50] P. Azaria, P. Lecheminant, and A. A. Nersisyan, *Phys. Rev. B* **58**, R8881 (1998).
- [51] S. Yan, D. A. Huse, and S. R. White, *Science* **332**, 1173 (2011).
- [52] H. C. Jiang, Z. Y. Weng, and D. N. Sheng, *Phys. Rev. Lett.* **101**, 117203 (2008).
- [53] S. Depenbrock, I. P. McCulloch, and U. Schollwöck, *Phys. Rev. Lett.* **109**, 067201 (2012).
- [54] Y.-C. He, D. N. Sheng, and Y. Chen, *Phys. Rev. Lett.* **112**, 137202 (2014).
- [55] H.-C. Jiang, H. Yao, and L. Balents, *Phys. Rev. B* **86**, 024424 (2012).
- [56] B. Bauer *et al.*, *Nat. Commun.* **5**, 5137 (2014).
- [57] A. Georges, G. Kotliar, W. Krauth, and M. J. Rozenberg, *Rev. Mod. Phys.* **68**, 13 (1996).
- [58] R. Suttner, C. Platt, J. Reuther, and R. Thomale, *Phys. Rev. B* **89**, 020408 (2014).
- [59] D. J. J. Farnell, O. Götze, J. Richter, R. F. Bishop, and P. H. Y. Li, *Phys. Rev. B* **89**, 184407 (2014).
- [60] S. Capponi, V. R. Chandra, A. Auerbach, and M. Weinstein, *Phys. Rev. B* **87**, 161118 (2013).
- [61] Y. Iqbal, F. Becca, and D. Poilblanc, *Phys. Rev. B* **84**, 020407 (2011).
- [62] Y. Iqbal, F. Becca, S. Sorella, and D. Poilblanc, *Phys. Rev. B* **87**, 060405 (2013); Y. Iqbal *et al.*, *Phys. Rev. B* **89**, 020407 (2014).
- [63] R. Kaneko, S. Morita, and M. Imada, *J. Phys. Soc. Jpn.* **83**, 093707 (2014).
- [64] J. B. Marston and C. Zeng, *J. Appl. Phys.* **69**, 5962 (1991).
- [65] M. B. Hastings, *Phys. Rev. B* **63**, 014413 (2000).

Gapless chiral spin liquid in a kagome Heisenberg model

Samuel Bieri,¹ Laura Messio,¹ Bernard Bernu,¹ and Claire Lhuillier¹

¹*Laboratoire de Physique Théorique de la Matière Condensée,
Université Pierre et Marie Curie, CNRS UMR 7600, F-75252 Paris, France*

(Dated: November 6, 2014)

In this Supplemental Material, we provide technical details and complementary information that were omitted in the main text of the paper.

A. Fermionic spinon mean fields and PSG classification

For completeness and to facilitate reproduction of results presented in the main text, we summarize here some key elements of the projective symmetry group (PSG) classification [1], and we remind a notation that is widely used in the literature.

The complex hopping ξ_{ij} and pairing Δ_{ij} parameters in the spinon Hamiltonian Eq. (3) of the main text are conveniently represented in the matrix form

$$u_{ij} = \begin{pmatrix} -\xi_{ij}^* & \Delta_{ij} \\ \Delta_{ij}^* & \xi_{ij} \end{pmatrix}. \quad (1)$$

The quadratic spinon Hamiltonian can be written using the $SU(2)_{\text{gauge}}$ doublet $\psi = (f_{\uparrow}, f_{\downarrow})^T$ as

$$H_0 = \sum_{i,j} \psi_i^\dagger u_{ij} \psi_j + h.c. \quad (2)$$

For spin-rotation invariant (singlet) liquids, we have $u_{ji} = u_{ij}^\dagger$ [2]. For the sake of brevity, we omit *on-site* terms (chemical potential and pairing) in the present discussion, but refer to the literature instead [1, 3].

Let g_j be a $SU(2)$ matrix on site j of the lattice. A local “gauge” transformation $\psi_j \mapsto g_j \psi_j$ in the spinon Hilbert space leaves the subspace of spin states ($n_j = f_\alpha^\dagger f_\alpha \equiv 1$) invariant. All transformations (space group or time reversal) acting in the spinon Hilbert space can therefore be supplemented by additional $SU(2)$ gauge rotations. The symmetry generators follow (lattice specific) algebraic relations, and their $SU(2)$ gauge representation must be compatible with these relations. The classification of algebraic PSG consists in listing all gauge-inequivalent symmetry representations that are compatible with these algebraic relations.

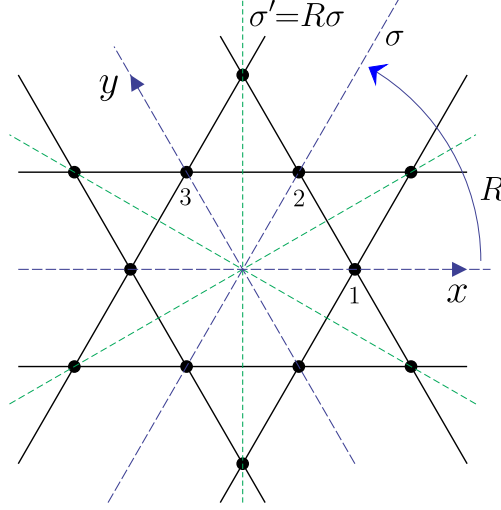


FIG. 1. Point group generators R and σ of the kagome lattice. The reflection symmetry $\sigma' = R\sigma$ is also shown, as well as translations in x and y direction. The sites labelled by 1, 2, 3 are chosen as a unit cell of the lattice.

B. Symmetries of the kagome lattice and their SU(2) representation

The point group generators, σ (reflection) and R (rotation by $\pi/3$), as well as translations x and y of the kagome lattice, as used in the main text, are illustrated in Fig. 1. For the unit cell, we choose the sites 1, 2, and 3 shown in the same figure. The reflection symmetry $\sigma' = R\sigma$ used in the main text is also shown.

The PSG representation of lattice symmetries can be written in the form

$$g_x(x, y) = \mathbb{1}_2, \quad (3a)$$

$$g_y(x, y) = (\epsilon_2)^x \mathbb{1}_2, \quad (3b)$$

$$g_\sigma(x, y) = (\epsilon_2)^{xy} g_\sigma, \quad (3c)$$

$$g_R(x, y) = (\epsilon_2)^{xy+y(y+1)/2} g_R, \quad (3d)$$

where x and y are the sublattice coordinates shown in Fig. 1. The sign $\epsilon_2 = \pm$ and the constant matrices g_σ and g_R are given in Tab. I of the main text for the gauge inequivalent PSG solutions of interest.

The matrix of mean-field parameters (1) on a given link (ij) may be propagated to another link using symmetry operations. At this point, the PSG representation enters the scene. For example, rotation R acts in the following way on the mean-field,

$$R(u_{ij}) = g_R(i) u_{R^{-1}(i)R^{-1}(j)} [g_R(j)]^\dagger. \quad (4)$$

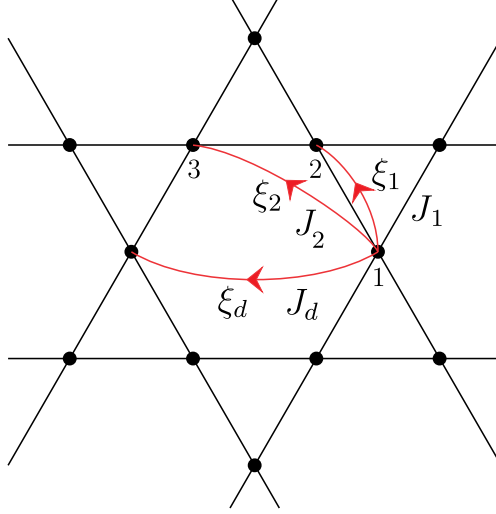


FIG. 2. Hopping parameters ξ_a on first, second, and diagonal lattice links as used in the main text. The propagation of these parameters to the entire lattice is then done using the algebraic PSG. The exchange interactions J_1 , J_2 , and J_d as used in Eq. (1) of the main text are also given.

Since the mean field u_{ij} must respect all lattice symmetries (up to time reversal and gauge transformations), u_{ij} on the rotated link can be identified with u_{ij} on the unrotated link. Time reversal is implemented in the spinon Hilbert space as $\Theta(u_{ij}) = -u_{ij}$ [4]. For the rotation symmetry R , we therefore find

$$u_{ij} = (-)^{\tau_R} g_R(i) u_{R^{-1}(i)R^{-1}(j)} [g_R(j)]^\dagger, \quad (5)$$

where $\tau_R \in \{0, 1\}$ is the time-reversal parity under rotation in the chiral spin liquid state, as discussed in the main text of the paper. Similarly, the mean field can be propagated by translation, using Eqs. (3a) and (3b).

The choice of hopping mean fields on first, second, and diagonal lattice links are displayed in Fig. 2. For U(1) liquids, there is always a gauge where the pairing $\Delta_{ij} = 0$. The complex hopping phases allowed by the symmetry constraints are given in Tab. I of the main text. To construct the spinon Hamiltonian on the entire lattice, it is convenient to start by rotating these mean fields around the hexagon using the PSG representation of R as discussed above. Finally, the rotated mean fields can be propagated to the entire lattice by translation in a similar way.

C. Spinon Fermi surface of CSL A

The lowest spinon mean-field band for CSL A is displayed in Fig. 3, for the optimal parameters at exchange coupling $J = (0.4, 0.1, 0.5)$; (describing kapellasite). The color code is such that the

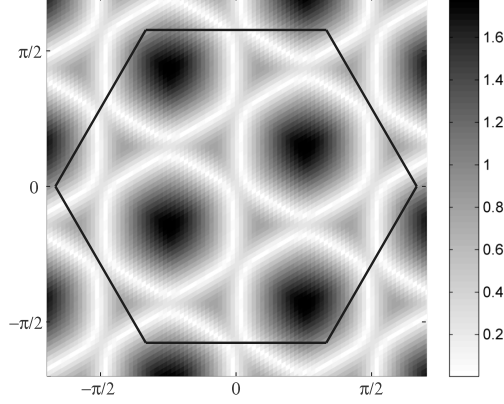


FIG. 3. Energy E (in meV) of the lowest spinon mean-field band in CSL A for the optimal parameters $\xi = (0.2, 2.7, 7.4)$ and hopping phases $\beta = (0.5, 0.2, 0.5)\pi$ at $J = (0.4, 0.1, 0.5)$. The spinon bandwidth is 2.1 meV. White lines are spinon Fermi surfaces ($E = 0$), and the black hexagon is the Brillouin zone.

white lines represent the spinon Fermi surfaces. The first Brillouin zone of the lattice is shown in black. Note that $\epsilon_2 = -1$ in this PSG (no. 13 in Tab. I of the main text) means that the spinon unit cell is doubled, and it contains 6 lattice sites. This translation (and rotation) symmetry breaking in the spinon spectrum is only a gauge artefact, and all physical quantities (spectral functions, two-spinon excitations, etc) respect those symmetries (see also [5]). The mean-field bandwidth in Fig. 3 is scaled to the energy cost of a projected spin $S = 1$ excitation, going from the Fermi surface to the highest spinon band ($\simeq 2.1$ meV).

D. Gutzwiller projection

In this study, the Gutzwiller projector in the construction of the QSL wave functions is crucial. At the quadratic mean-field level (i.e., without Gutzwiller projection) and for a spin-rotation invariant QSL, one can show that the two-point function is given by

$$\langle \mathbf{S}_i \cdot \mathbf{S}_j \rangle_{\text{MF}} = -\frac{3}{8}(|\langle \hat{\chi}_{ij} \rangle|^2 + |\langle \hat{\eta}_{ij} \rangle|^2) \quad (6)$$

in the standard notation $\hat{\chi}_{ij} = f_{i\alpha}^\dagger f_{j\alpha}$ and $\hat{\eta}_{ij} = \varepsilon_{\alpha\beta} f_{i\alpha} f_{j\beta}$ [1]. That is, the spin correlators are never ferromagnetic in a mean-field approach of Abrikosov fermions. This fact is to be contrasted with Schwinger boson mean-field theory [6–8], where hopping gives ferromagnetic correlators, while pairing results in anti-ferromagnetic ones.

The highly accurate approximation of ground state (and low-lying excitations) of the anti-ferromagnetic Heisenberg spin-1/2 chain by fermionic spinons [9, 10] is only achieved once the Gutzwiller projector is applied to the Slater determinant. Only then, the staggered nature of

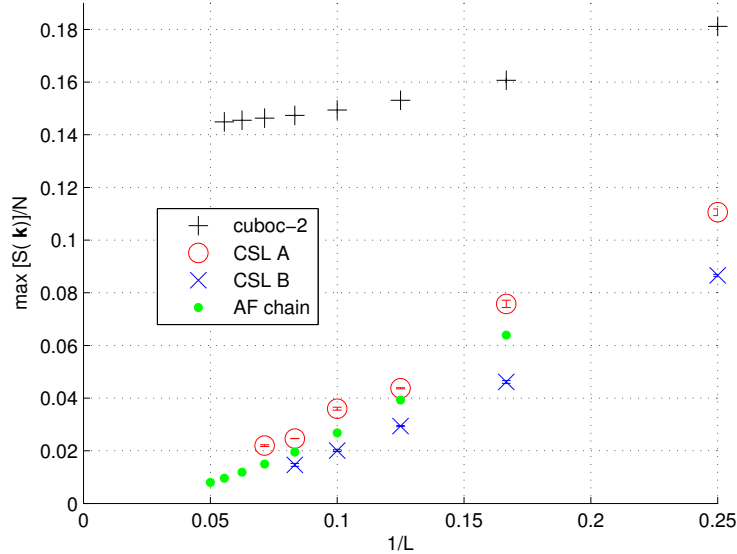


FIG. 4. Scaling of the peaks $\max[S(\mathbf{k})]/N$ as a function of $1/L$ for the three QSL phases and for the semi-classical cuboc-2 phase discussed in this paper. The CSL states have fixed variational parameters, as given in the main text; CSL A: $\xi = (0.2, 2.7, 7.1)$, $\beta = (0.5, 0.2, 0.5)$; CSL B: $\xi = (2.4, 0.2, 7.4)$, $\beta = (0.2, 0.5, -0.04)\pi$.

the correlation function and the correct long-distance power law are recovered, $S(x) \propto (-)^x/|x|$. It is therefore no surprise that Gutzwiller projection has strong effects on the two-dimensional QSL states discussed in this paper. For instance, in the limit of decoupled arrays of chains, the unphysical inter-chain scattering of mean-field spinons is merely suppressed by the projection.

E. Ordered moments

The attentive reader may be worried that the pronounced peaks in the spin structure factors $S(\mathbf{k})$ for the QSL phases displayed in Fig. 3 of the main text could indicate a symmetry breaking and long-range ordering as the system size grows. In fact, for the anti-ferromagnetic (AF) spin chain, it is known that the structure factor at the AF wave vector diverges logarithmically with system size. In Fig. 4, we display a finite-size scaling of the ordered moment for the QSL phases discussed in the main text. We conclude from this analysis that the peaks in the 2D CSL phases are at most logarithmically divergent, and these phases do not exhibit translation symmetry breaking.

For comparison, we also display the ordered moment of the semi-classical cuboc-2 state in Fig. 4 for parameters close to the transition line, $J \simeq (0.4, 0.1, 0.5)$. The ordered moment of this wave function is clearly finite in the thermodynamic limit, with a magnitude of approximately 80% of

the classical value. It should be noted that while the relatively simple Huse-Elser wave functions we use in this study [Eq. (2) of the main text] provide good estimates of the ground state energy, it is known that the ordered moment is generally overestimated in this approach (see, e.g., [11] and refs. therein).

-
- [1] X.-G. Wen, Phys. Rev. B **65**, 165113 (2002).
 - [2] Here, spin rotation is represented non-projectively in the spinon space, simply by $(f_{\uparrow}, f_{\downarrow})^T \mapsto U(f_{\uparrow}, f_{\downarrow})^T$, where U is the SU(2) rotation matrix. Recently, a *projective* representation of spin rotation was proposed in Ref. [12] which results in a slightly more refined classification.
 - [3] We note that on-site terms are present in our spinon Hamiltonian. If allowed by symmetry, they are consistently adjusted to bring the wave function to half filling before Gutzwiller projection. For the U(1) CSL A and CSL B states of this paper, it turns out that the chemical potentials are pinned to zero by symmetries.
 - [4] The choice $\Theta(u_{ij}) = -u_{ij}$ for the TRS representation is not crucial for main results of this paper. Furthermore, we would like to stress that time reversal does not enter the algebraic PSG classification.
 - [5] Y. Ran, M. Hermele, P. A. Lee, and X.-G. Wen, Phys. Rev. Lett. **98**, 117205 (2007); M. Hermele *et al.*, Phys. Rev. B **77**, 224413 (2008).
 - [6] S. Sachdev, Phys. Rev. B **45**, 12377 (1992).
 - [7] F. Wang and A. Vishwanath, Phys. Rev. B **74**, 174423 (2006).
 - [8] L. Messio, B. Bernu, and C. Lhuillier, Phys. Rev. Lett. **108**, 207204 (2012); L. Messio, C. Lhuillier, and G. Misguich, Phys. Rev. B **87**, 125127 (2013).
 - [9] S. Yunoki and S. Sorella, Phys. Rev. B **74**, 014408 (2006).
 - [10] B. S. Shastri, Phys. Rev. Lett. **60**, 639 (1988); F. D. M. Haldane, Phys. Rev. Lett. **60**, 635 (1988).
 - [11] P. H. Y. Li, R. F. Bishop, and C. E. Campbell, arXiv:1410.6003.
 - [12] G. Chen, A. Essin, and M. Hermele, Phys. Rev. B **85**, 094418 (2012).